ISSN 1027-4510, Journal of Surface Investigation: X-ray, Synchrotron and Neutron Techniques, 2023, Vol. 17, No. 6, pp. 1199–1206. © Pleiades Publishing, Ltd., 2023.
Russian Text © The Author(s), 2023, published in Poverkhnost', 2023, No. 11, pp. 24–32.

Effect of Aluminum on the Structure and Electrical Properties of Amorphous Diamond-Like Silicon-Carbon Films

A. I. Popov[a, b, *], A. D. Barinov[a, b, **], V. M. Yemets[a], D. A. Zezin[a, b], T. S. Chukanova[a], V. P. Afanas'ev[a], M. A. Semenov-Shefov[a], V. A. Terekhov[c], E. P. Domashevskaya[c], M. Yu. Presnyakov[d], and M. A. Shapetina[e]

[a] *National Research University "Moscow Power Engineering Institute," Moscow, 111250 Russia*
[b] *Institute of Nanotechnology of Microelectronics, Russian Academy of Sciences, Moscow, 119991 Russia*
[c] *Voronezh State University, Voronezh, 394018 Russia*
[d] *National Research Center "Kurchatov Institute," Moscow, 123182 Russia*
[e] *Moscow State Pedagogical University, Moscow, 119991 Russia*
**e-mail: popovai2009@gmail.com*
***e-mail: barinovad@mpei.ru*

Received December 21, 2022; revised February 20, 2023; accepted February 20, 2023

Abstract—The effect of a metal that weakly forms carbides, i.e., aluminum, on the phase composition, structure, and electrophysical properties of amorphous diamond-like silicon-carbon films is studied. The obtained results are compared with the influence of carbide-forming transition metals, titanium and hafnium, on the same characteristics. It is shown that the effect of aluminum and transition metals on the structure and properties of silicon–carbon films is fundamentally different. The introduction of aluminum in a wide range of concentrations, in contrast to transition metals, does not lead to the formation of a nanocrystalline phase in the films. The concentration dependences of the electrical conductivity upon the introduction of aluminum have a smooth, monotonic character, but upon the introduction of transition metals, they have a pronounced percolation character, and the absolute values of changes in the electrical conductivity differ by orders of magnitude. The set of studies carried out makes it possible to conclude that the reason for these differences is the interaction of the introduced metals with different chemical elements of the film. Transition-metal atoms interact mainly with carbon atoms to form highly conductive carbide nanocrystals. In contrast, aluminum atoms mainly interact with oxygen atoms and form an amorphous phase of aluminum oxide.

Keywords: amorphous silicon–carbon films, aluminum, transition metals, structure, phase composition, electrical conductivity, dielectric losses

DOI: 10.1134/S1027451023060174

INTRODUCTION

Amorphous diamond-like silicon—carbon films obtained by the decomposition of organosilicon precursors contain, along with carbon atoms, a significant amount of silicon and oxygen atoms. Their presence in the structural network reduces mechanical stresses in a material and increases the stability of the amorphous state [1]. In turn, a reduction in stresses improves the adhesion of these films compared to widely used diamond-like films of amorphous carbon; the high stability of the amorphous state of the initial silicon–carbon structural network makes it possible to introduce a large amount of impurities into them (for example, metals of more than 30 at % [2]) while maintaining the amorphous state of the initial silicon–carbon structural network. The latter makes it possible to control various material properties over a wide range, which ensures the creation of coatings with the necessary mechanical, tribological [3, 4], biological [5], electrical [6, 7], and other properties. It was shown in [8] that the use of methods of structural and chemical modification of the properties of diamond-like silicon–carbon films made it possible to change their electrical conductivity by 12 orders of magnitude. As elements for modifying silicon–carbon films, as a rule, transition metals are used, which form carbides well. In the process of creating such compounds, a nanocomposite structure arises consisting of a dielectric amorphous matrix and metal-carbide nanocrystals with high electrical conductivity. At the same time, the influence of other groups of metals on the properties of silicon–carbon films has not been sufficiently studied. In the present work, the influence on the structure and properties of amorphous diamond-like silicon–carbon films of a metal with a low affinity for carbon, namely aluminum, is studied. The

obtained results are compared with those for transition metals: titanium and hafnium.

EXPERIMENTAL

Metal-containing amorphous diamond-like silicon–carbon films prepared by the plasma-chemical decomposition of polyphenylmethylsiloxane (PPMS) [9] in an alternating electric field with simultaneous magnetron sputtering of the metal using the setup described in [10] were the objects of study. The frequency of the electric field was 112 kHz. Polyphenylmethylsiloxane consists of chain molecules $(CH_3)_3Si[CH_3C_6H_5SiO]_nOSi(CH_3)_3$, which have a structure asymmetric about the chain axis with branches in the form of phenyl and CH_3 groups. It was shown in [11] that silicon–carbon films obtained by the plasma-chemical decomposition of polyphenylmethylsiloxane contain molecules or, at least, fragments of molecules of polyphenylmethylsiloxane. To obtain metal-containing films, magnetron sputtering of the metal is carried out simultaneously with the plasma-chemical decomposition of polyphenylmethylsiloxane. In this case, depending on the position of the substrates relative to the plasmotron and magnetron, it is possible to obtain a set of samples with different metal content in a single technological cycle. The samples were fabricated on single-crystal silicon and metal substrates. In the latter case, an aluminum electrode was formed on the film surface to carry out electrophysical measurements. The thickness of the films was from 1 to 3 μm.

The structure, phase, and elemental composition of the samples were studied using high-resolution electron microscopy and diffraction on a STEM/TEM Titan 80-300 transmission electron microscope and using X-ray spectral analysis on a Vega II SBU scanning electron microscope with an Inca x-Act energy-dispersive detector. X-ray spectroscopy was carried out by two methods: using X-ray photoelectron spectroscopy (XPS) on Versa ProbeII ULVAC-PHI and Kratos Axis Ultra DLD setups and using ultra-soft X-ray emission spectroscopy on a PCM-500 X-ray spectrometer monochromator.

Studies of the electrophysical and dielectric properties at different temperatures were carried out using a Novocontrol Alpha-A setup for complex measurement of the dielectric properties of materials and an ASEC-03E automated system for electrophysical measurements. The studies were carried out at voltages from 1 to 5 V corresponding to the ohmic region of the current–voltage characteristics.

ELECTRON MICROSCOPY AND DIFFRACTION

Figure 1 shows the dependence of the chemical composition of silicon–carbon films on the content of aluminum in them in a wide range of concentrations of the latter. It can be seen that an increase in the concentration of aluminum in the films leads mainly to a decrease in the content of carbon in them, but the concentrations of silicon and oxygen changes much less. Since the operation of the magnetron during the production of metal-containing films necessitates the presence of argon in the working chamber, the concentration of the latter in the samples was also controlled, but it was less than 1% in the films.

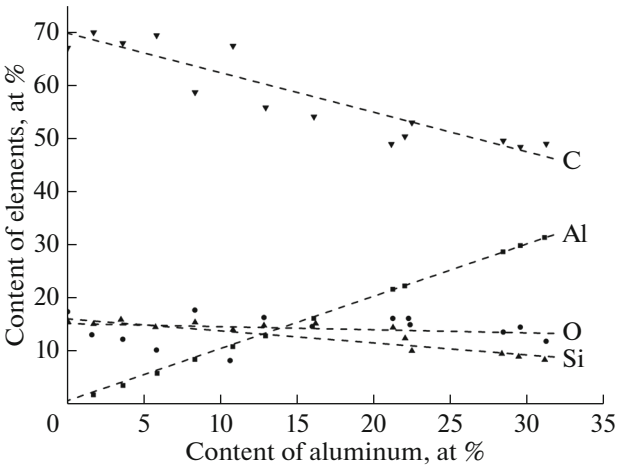

Fig. 1. Dependence of the concentration of the main chemical elements in silicon–carbon films on the aluminum content.

To determine the phase composition of aluminum-containing silicon–carbon films, studies were carried out using high-resolution transmission electron microscopy (HRTEM) and electron diffraction. Figures 2a and 2b show examples of HRTEM images of a cross section of silicon-carbon films with 18 at % of aluminum at different magnifications. For comparison, Fig. 2c shows a typical image of a cross section of a film with 15 at % of transition metal (titanium). The insets show the diffraction patterns obtained from these samples.

From a comparison of Figs. 2a–2c, it can be seen that the behavior of aluminum and titanium in amorphous diamond-like silicon–carbon films is fundamentally different. There is no nanocrystalline phase in aluminum-containing films in the entire studied range of metal concentrations. Even in the atomic resolution mode (Fig. 2b), there are no regions with an ordered arrangement of atoms (nanocrystals) in the samples. The absence of a crystalline phase at all aluminum concentrations is also confirmed by the results of diffraction studies: the diffraction patterns are diffuse halos typical of the amorphous phase.

In contrast, when transition metals (titanium, hafnium [12], molybdenum [7], tantalum [13], and others) are introduced into silicon–carbon films at metal concentrations above 2–4 at %, a crystalline phase of metal carbide with a crystal size of several nanometers

is observed in amorphous films. In the image of a cross section of a silicon–carbon film with 15 at % of titanium (Fig. 2c), regions with an ordered arrangement of atoms (nanocrystals) are visible. The electron-diffraction patterns from these regions have rather pronounced reflections. The minimum concentration of metal, at which nanocrystals are observed, is determined by the size of the latter and is different for different metals [7].

An analysis of the electron-diffraction patterns obtained from nanocrystals in films containing transition metals (titanium, hafnium, molybdenum, and tungsten), as well as the Fourier analysis of images of nanocrystals in tantalum-containing films [7, 12, 13], showed that the nanocrystals are metal carbide with the chemical formula *Me*C in all cases.

X-RAY SPECTROSCOPY

As shown above, studies of silicon-carbon films with metals using high-resolution electron microscopy together with diffraction studies showed the absence of any crystalline inclusions in films with aluminum and the formation of metal-carbide nanocrystals when a transition metal is introduced into the film. To obtain information about the chemical bonds that arise when aluminum atoms are introduced into silicon–carbon films, the samples were studied using XPS. For comparison, analogous studies of films with titanium were carried out in the same modes at close concentrations of the metal.

Figure 3a shows the photoelectron spectra of a silicon–carbon film with 2.18 at % of titanium. Overview XPS spectra (Fig. 3a) were obtained immediately after placing the sample in the setup and after removing the surface layer by etching the samples with argon ions (the ion energy was 2 keV, the size of the cleaning region was 2 × 2 mm) until the chemical composition of the samples stabilized. As can be seen from comparison of the spectra, surface etching resulted in the appearance of a number of additional peaks and a change in the intensities of some existing peaks (for example, carbon), which is due to cleaning. Further in this work, the XPS spectra of the samples after surface etching are shown.

Figure 3b shows the high-resolution spectrum in the range of binding energies of carbon atoms C 1*s*. Figure 3a also shows the peak positions for the binding energy in pure carbon and in TiC and SiC compounds [14]. As can be seen from the figure, the C 1*s* peak in the sample under study is shifted with respect to the peak of pure carbon to the region of lower energies, where the peaks of titanium carbide and silicon carbide are located. The peak in the range of binding energies of titanium atoms Ti 2*p* (Fig. 3c) is also shifted with respect to the peak of pure titanium towards the position of the TiC peak. The data presented are consistent with the results of studies using

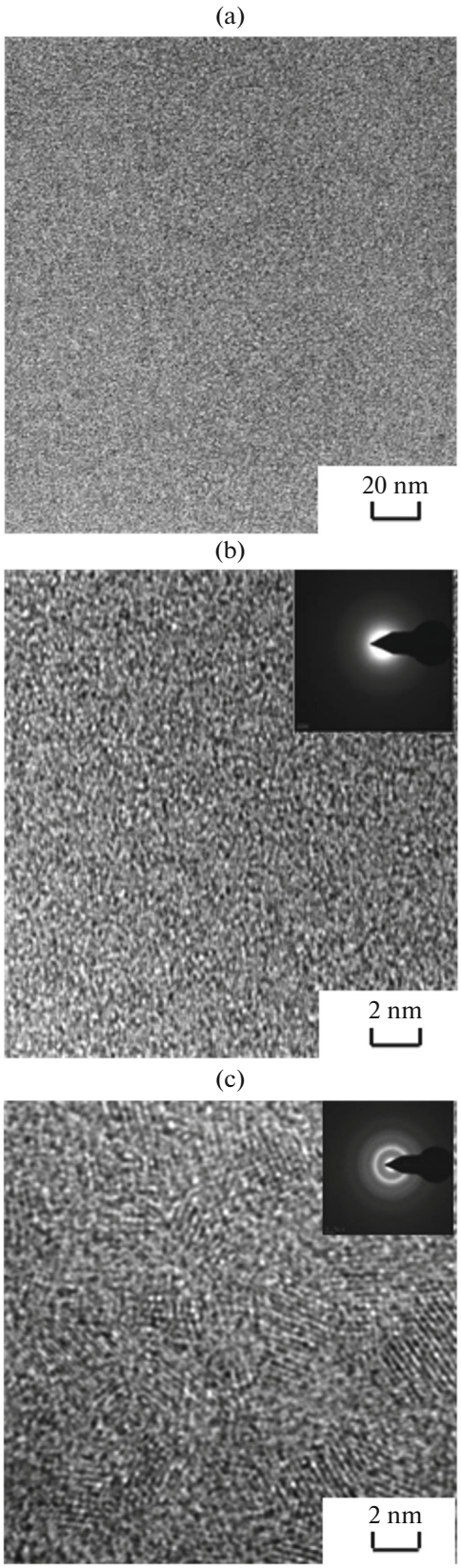

Fig. 2. HRTEM images of a cross section of silicon–carbon films (a and b) with 18 at % of aluminum with different magnifications and (c) with 15 at % of titanium. The insets show the corresponding electron-diffraction patterns.

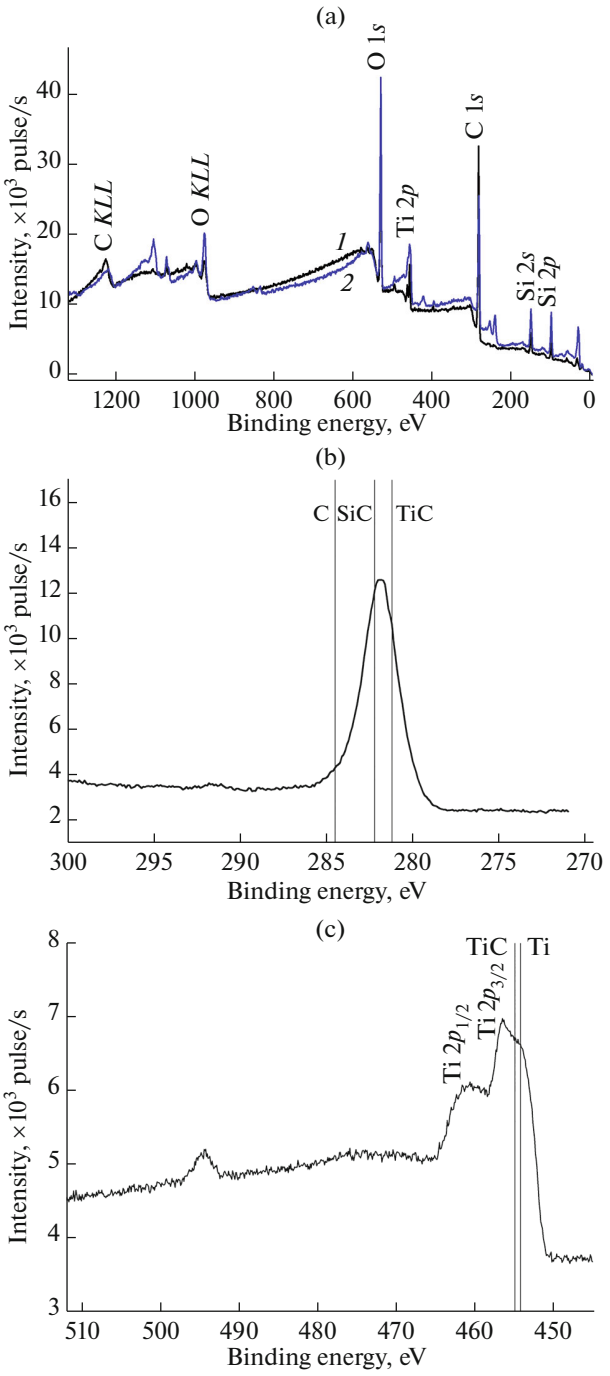

Fig. 3. (a) Overview XPS spectrum and spectra in the range of binding energies of (b) carbon atoms C 1*s* and (c) titanium atoms Ti 2*p* of a sample containing 2.18 at % of Ti (*1*) before and (*2*) after cleaning with argon ions.

electron microscopy and indicate that when atoms of the transition metal (titanium) are introduced into the silicon–carbon film, they form chemical bonds with carbon atoms.

Similar results were obtained when other transition metals, such as tantalum, molybdenum, and hafnium, were introduced into diamond-like silicon–carbon films. It was shown in [15] that tungsten is a partial exception to this rule; its introduction results in the formation of both tungsten-carbide nanocrystals and the amorphous phase of tungsten oxide.

As mentioned above, in contrast to transition metals, the introduction of up to 25 at % of aluminum does not lead to the formation of a crystalline phase. Figure 4a shows the XPS results for films with aluminum (3.66 at % of Al). The Al 2*p* peak (Fig. 4b) has a relatively large width (69–75 eV) and an irregular shape, which indicates that it consists of several signals. In the energy range, at which this peak is located, the binding energies of pure aluminum, aluminum oxide, and aluminum carbide are located. However, the peak shape does not satisfy the Rayleigh criterion. In this regard, it is not possible to reliably separate components of this peak, and, accordingly, to determine the chemical bonds of aluminum atoms.

The C 1*s* peak is shifted relative to the binding energy in pure carbon to lower energies and the position of its maximum is close to the binding energies of carbon in silicon carbide (282.5 eV) and aluminum carbide (282.4 eV) (Fig. 4c). Therefore, on the basis on the position of the C 1*s* peak, it is impossible to reliably determine, which of the two mentioned types of bonds it corresponds to.

The position of the O 1*s* peak (Fig. 4d) is in the region of the binding energy in aluminum oxides, which allows one to conclude that aluminum oxide is present in the object under study. Some shift of the peak relative to the binding energy in Al_2O_3 may be due to the presence in the sample of oxides of nonstoichiometric composition AlO_x with $x < 1.5$.

Thus, the results of XPS studies indicate that when transition-metal atoms are introduced into the film, the latter interact with carbon atoms from the initial silicon–carbon network to form the corresponding carbides. In contrast, in films containing aluminum, an aluminum-oxide phase is formed. At the same time, the results of XPS do not make it possible to reliably determine the presence or absence of aluminum–carbon compounds in these films. To answer this question, samples were studied by ultra-soft X-ray emission spectroscopy. Films with a rather high aluminum content (18 and 25 at % of Al) were studied. The X-ray emission $L_{2,3}$ spectra were obtained in the region of chemical binding energies of silicon and aluminum atoms (Fig. 5).

Figure 5a shows the X-ray emission spectra of Si $L_{2,3}$. To estimate the phase composition of the samples, the spectra of models with different ratios of the concentrations of chemical bonds between silicon and carbon and oxygen were calculated. The spectra of silicon carbide and silicon dioxide were used as reference ones. The best agreement with the experimental spectra was shown by models, in which 65–70% of silicon atoms form chemical bonds with carbon, and 30–35%

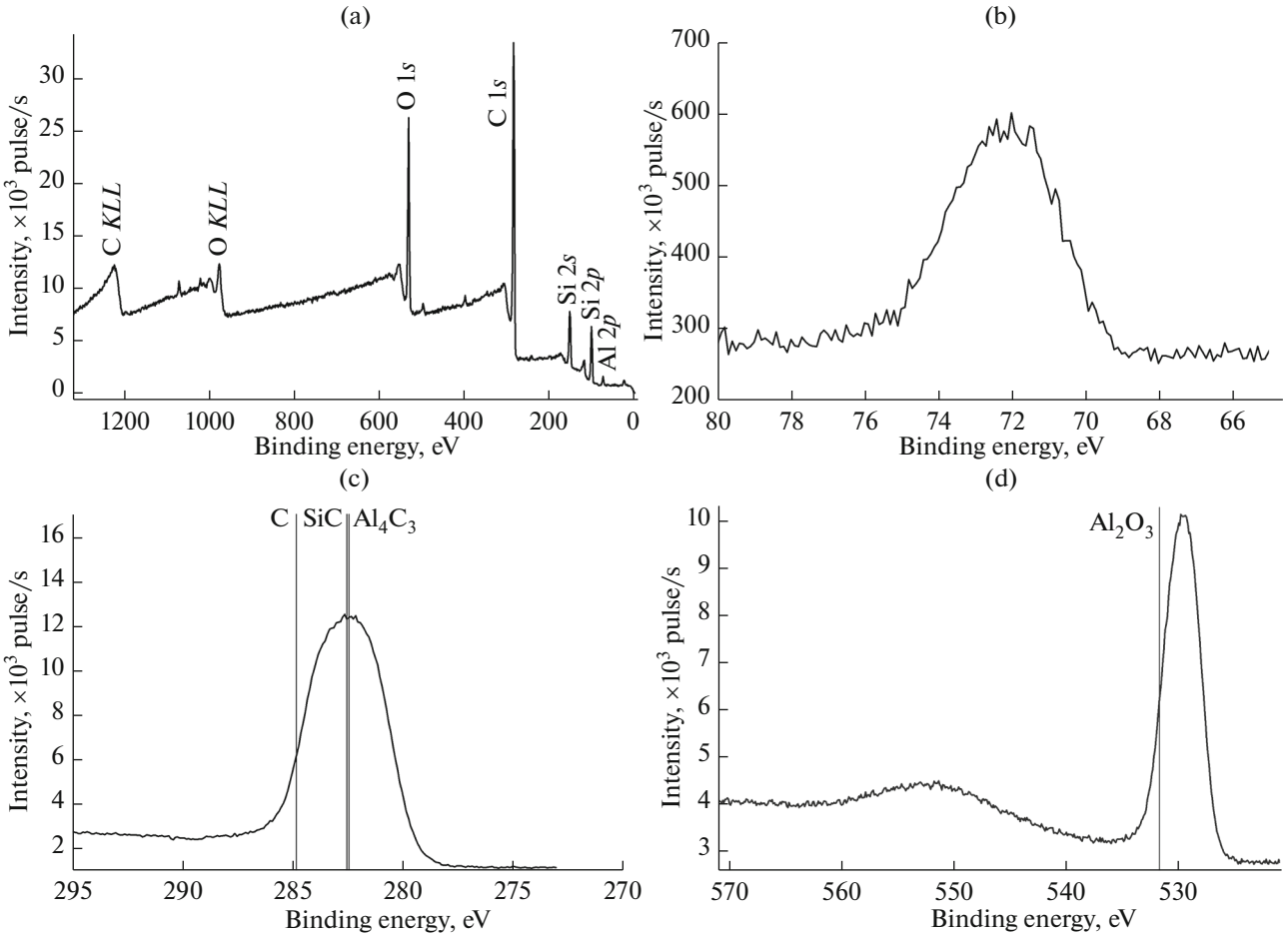

Fig. 4. (a) Overview XPS spectrum and spectra in the ranges of binding energies of (b) aluminum atoms Al 2*p*, (c) carbon atoms C 1*s*, and (d) oxygen atoms O 1*s* of a sample containing 3.66 at % of aluminum.

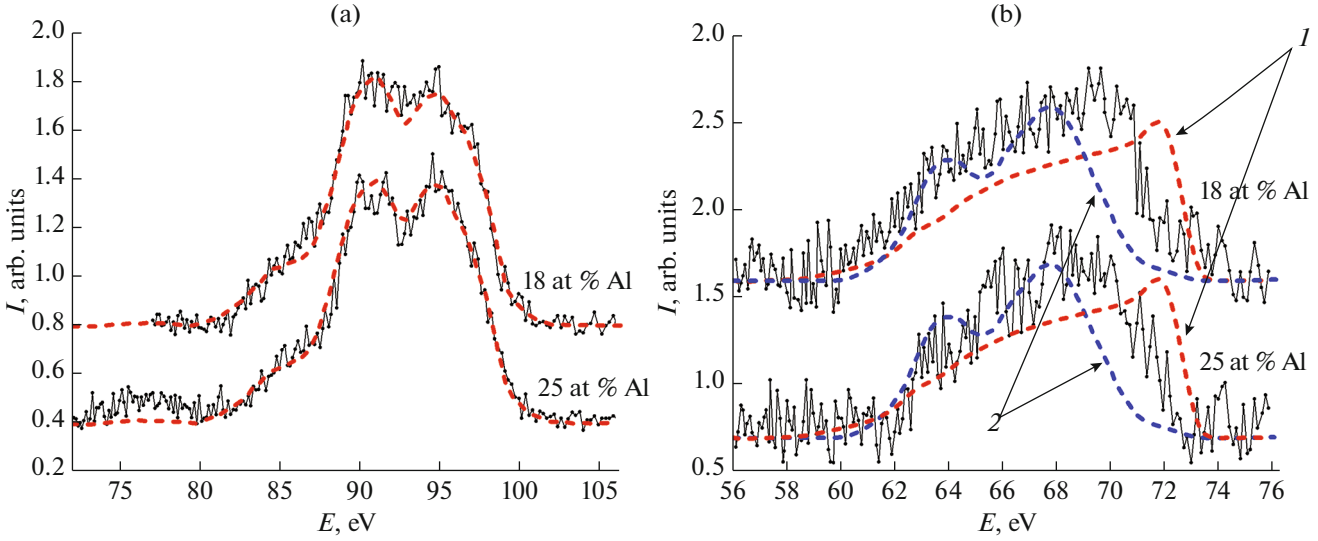

Fig. 5. X-ray emission $L_{2,3}$ spectra of aluminum-containing films in the energy range of chemical bonds of (a) silicon atoms and (b) aluminum atoms. The dotted lines show (a) the spectra of model samples, in which 65–70% of silicon atoms form chemical bonds with carbon and 30–35% of silicon atoms form chemical bonds with oxygen, and (b) the spectra of the reference samples of (*1*) pure Al and (*2*) Al_2O_3.

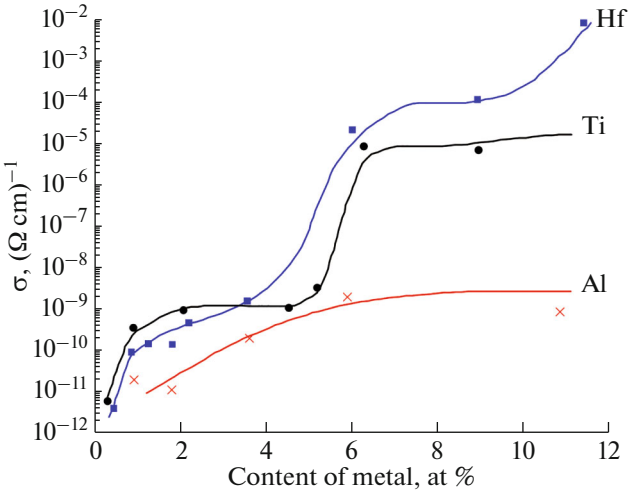

Fig. 6. Dependence of the electrical conductivity of silicon–carbon films σ on the concentration of titanium, hafnium, and aluminum in them.

of silicon atoms form chemical bonds with oxygen. The spectra of these models are shown in Fig. 5a with a dotted line. The error of the presented data calculated from the closeness of the experimental and calculated spectra from the model does not exceed 5%.

Figure 5b shows the X-ray emission spectra of Al $L_{2,3}$ for the reference samples of pure aluminum and Al_2O_3, as well as for the studied silicon–carbon films with aluminum. It follows from their comparison that the main maximum in the spectra of the studied samples is between the main maxima of the spectra of aluminum and Al_2O_3. This may be related to the presence of AlO_x oxides with $x \leq 1.5$ in the studied films.

Thus, the results of the X-ray spectroscopy of silicon–carbon films with aluminum allow one to draw a conclusion about the formation of chemical bonds of oxygen atoms with aluminum and silicon atoms with carbon and oxygen. However, none of the X-ray spectroscopy methods used gave unambiguous confirmation of the presence or absence of aluminum carbide in the films. On the other hand, the low affinity of carbon for aluminum [16], as well as the absence of aluminum-carbide peaks noted in [17] in the XPS spectra of amorphous carbon films with aluminum, allow one to assume with a high degree of probability that when aluminum is introduced into silicon–carbon films, no significant amount of Al–C chemical bonds is formed.

ELECTROPHYSICAL PROPERTIES

In addition to direct experiments, indirect methods, in particular, the study of the influence of a metal on the electrophysical properties of the material can provide information about the forms of metal incorporation into a silicon–carbon film. In this regard, let us compare the effect of aluminum and transition metals on the electrical conductivity and dielectric properties of amorphous diamond-like silicon–carbon films.

Figure 6 shows the concentration dependence of the electrical conductivity of aluminum-containing films. The same figure shows similar dependences for titanium- and hafnium-containing films from [12]. It can be seen that the behavior of the dependences for films with aluminum and films with transition metals radically differs from each other. The concentration dependences of films with transition metals have a pronounced percolation character. In contrast to this, the electrical conductivity of the films with aluminum steadily increases with increasing metal concentration. In addition to the type of dependences, the absolute values of changes in the electrical conductivity also differ. So, when the concentration of the transition metal changes from 1 to 11 at %, the electrical conductivity increases by 6–7 orders of magnitude. However, the same change in the concentration of aluminum causes an increase in the electrical conductivity only within two orders of magnitude.

An increase in the electrical conductivity with an increase in the concentration of the transition metal in silicon–carbon films in the region up to the percolation threshold is explained by an increase in the volume of the highly conductive metal-carbide phase and an increase in the density of localized states due to the borrowing of carbon atoms from the silicon–carbon structural network during the formation of metal carbides [18].

According to structural studies, the results of which are presented above, when aluminum is introduced into silicon–carbon films, an amorphous phase of aluminum oxide is formed. Since aluminum oxides are a dielectric, the formation of this phase cannot cause an increase in the electrical conductivity of the sample. On the other hand, the formation of aluminum oxides is accompanied by the removal of oxygen atoms from the silicon–carbon film. As noted above, silicon-carbon films contain molecules or fragments of molecules of polyphenylmethylsiloxane. The oxygen atoms in these molecules are bridging atoms connecting the repeating elements of the molecule. Therefore, the removal of oxygen atoms during the formation of aluminum oxides should lead to the defragmentation of silicon–carbon film molecules and, consequently, to an increase in dangling bonds and concentration of localized states. In turn, taking into account the hopping nature of the conductivity in the objects under study [19], an increase in the concentration of localized states in the tails of the bands leads to an increase in the electrical conductivity.

Studies of the dielectric properties of metal-containing films showed that with an increase in the aluminum concentration above 1–2 at %, the real part of the permittivity increases just as it was observed in the case of transition metals in the same concentration

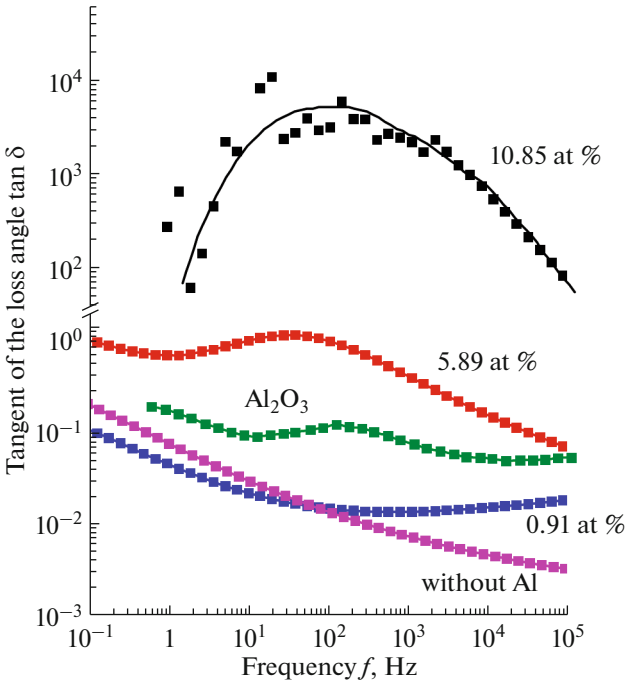

Fig. 7. Frequency dependences of the tangent of the dielectric-loss angle of silicon–carbon films at different concentrations of aluminum and Al_2O_3 film.

range [12]. It should be noted that in both cases the rate of increase grows with decreasing frequency of measurements. This type of dependence is typical for materials with relaxation polarization. Figure 7 shows the frequency dependences of the tangent of the dielectric-loss angle of silicon–carbon films with an aluminum content of 0.91, 5.89, and 10.85 at % at room temperature. The same figure shows the dependences for a metal-free film [12] and for an Al_2O_3 film (at 50°C) [20]. As can be seen from Fig. 7, the addition of 0.91 at % of aluminum slightly increases the tangent of the dielectric-loss angle in the frequency range from 10^3 to 10^6 Hz. The addition of 5.89 at % of aluminum to the film leads to an increase in the tangent of the dielectric-loss angle over the entire frequency range and to the appearance of a wide maximum in the region from 20 to 200 Hz. Growth in the concentration of aluminum to 10.85 at % causes a significant increase in the absolute values of the tangent of dielectric-loss angle, and the maximum at frequencies of 30–50 Hz becomes more pronounced.

Comparing the described curves obtained at room temperature with the curve for Al_2O_3 obtained in [20] at 50°C, one can note the close position of the considered maxima. And taking into account that, according to the data of [20], with increasing temperature, the position of the maximum shifts towards higher frequencies, it can be argued that the maximum observed at 20°C for silicon–carbon films with aluminum and the maximum on the curve for the Al_2O_3 film are due to the same type of relaxers. Significantly higher values of the tangent of the dielectric-loss angle of the films at a high aluminum content, as compared to Al_2O_3, are explained both by an increase in the through-conduction currents due to an increase in the electrical conductivity of the material, and by an increase in the concentration of relaxers due to the defragmentation of molecules upon the removal of oxygen atoms from them.

Thus, studies of the dielectric properties of aluminum-containing silicon–carbon films also confirm the formation of an oxide phase in them.

CONCLUSIONS

The studies carried out showed that the effect of aluminum and transition metals on the structure and electrophysical properties of amorphous diamond-like silicon–carbon films is fundamentally different. Thus, the introduction of aluminum into these objects does not lead to the formation of a nanocrystalline phase in them over the entire range of concentrations studied. In the case of the introduction of transition metals at concentrations above 2–4 at %, crystals with a size of a few nanometers appear in the films. The reason for these differences is that transition-metal atoms interact mainly with carbon atoms taking them from the initial structural network of the film with the formation of metal-carbide nanocrystals. In contrast, when aluminum is introduced, metal atoms interact mainly with oxygen present in the structural network with the formation of an amorphous phase of aluminum oxide AlO_x with $x \le 1.5$.

Differences in the structure and phase composition of the films, in turn, determine the electrophysical properties of the materials. The dependences of the electrical conductivity of the films on the concentration of the considered metals differ both qualitatively and quantitatively. In the case of transition metals, these dependences have a pronounced percolation character with changes in the absolute values of the electrical conductivity (in the case of titanium and hafnium) by 6–7 orders of magnitude with an increase in the metal concentration to 10–11 at %. In the case of the introduction of aluminum, the concentration dependences of the electrical conductivity have a smooth, monotonic character with a change in the absolute values within the limit of two orders of magnitude in the same concentration range. These changes are related to an increase in the density of localized states in the silicon—carbon structural network due to the removal of oxygen atoms as a result of the formation of the AlO_x oxide phase. The formation of aluminum oxide in aluminum-containing films is also confirmed by the results of studying the dielectric properties of the material. On the frequency dependences of the tangent of the dielectric-loss angle of samples with an aluminum content of more than 5 at %,

a maximum is observed at frequencies close to that at which the maximum is located on a similar dependence for aluminum oxide.

FUNDING

The study was supported by the Russian Science Foundation, grant no. 22-29-00864, https://rscf.ru/project/22-29-00864/.

CONFLICT OF INTEREST

The authors declare that they have no conflicts of interest.

REFERENCES

1. Š. Meškinis and A. Tamulevičien'e, Mater. Sci. **17**, 358 (2011). https://doi.org/10.5755/j01.ms.17.4.770
2. C. Vencatraman, A. Goel, R. Lei, D. Kester, and C. Outten, Thin Solid Films **308–309**, 173 (1997). https://doi.org/10.1016/S0040-6090(97)00384-2
3. F. Mangolini, B. A. Krick, T. D. B. Jacobs, S. R. Khanal, F. Streller, J. B. McClimon, J. Hilbert, S. V. Prasad, T. W. Scharf, J. A. Ohlhausen, J. R. Lukes, W. G. Sawyer, and R. W. Carpick, Carbon **130**, 127 (2018). https://doi.org/10.1016/j.carbon.2017.12.096
4. E. V. Zavedeev, O. S. Zilova, M. L. Shupegin, A. D. Barinov, N. R. Arutyunyan, T. Roch, and S. M. Pimenov, Appl. Phys. A **122**, 961 (2016). https://doi.org/10.1007/s00339-016-0508-7
5. D. Bociaga, A. Sobczyk-Guzenda, W. Szymanski, A. Jedrzejczak, A. Jastrzebska, A. Olejnik, L. Swiatek, and K. Jastrzebski, Vacuum **143**, 395 (2017). https://doi.org/10.1016/j.vacuum.2017.06.027
6. M. A. Velichko and Yu. P. Gladkikh, Nauchn. Ved. Belgorod. Nauchno-Issled. Univ., Ser. Mat. Fiz., No. 6 (227), 115 (2016).
7. A. D. Barinov, A. I. Popov, and M. Yu. Presnyakov, Inorg. Mater. **53**, 690 (2017). https://doi.org/10.1134/S0020168517070019
8. A. I. Popov, A. D. Barinov, and M. Y. Presniakov, J. Nanoelectron. Optoelectron. **9**, 787 (2015). https://doi.org/10.1166/jno.2014.1678
9. V. D. Frolov, S. M. Pimenov, E. V. Zavedeev, V. I. Konov, E. N. Lubnin, and G. G. Kirpienko, J. Surf. Invest.: X-ray, Synchrotron Neutron Tech. **1**, 303 (2007). https://doi.org/10.1134/S1027451007030135
10. M. L. Shupegin, Zavod. Lab., Diagn. Mater. **79** (2), 28 (2013).
11. A. I. Belogorokhov, A. M. Dodonov, M. D. Malinkovich, Yu. N. Parkhomenko, A. P. Smirnov, M. L. Shupegin, Izv. Vyssh. Uchebn. Zaved., Mater. Elektron. Tekh., No. 1, 69 (2007).
12. A. I. Popov, A. D. Barinov, V. M. Emets, R. A. Kastro Arta, A. V. Kolobov, A. A. Kononov, A. V. Ovcharov, and T. S. Chukanova, Phys. Solid State **64**, 85 (2022). https://doi.org/10.1134/S1063783422010164
13. M. Yu. Presniakov, A. I. Popov, D. S. Usol'tseva, M. L. Shupegin, and A. L. Vasil'ev, Nanotechnol. Russ. **9**, 518 (2014). https://doi.org/10.1134/S1995078014050139
14. A. V. Naumkin, A. Kraut-Vass, S. W. Gaarenstroom, and C. J. Powell, NIST X-Ray Photoelectron Spectroscopy Database, ver. 1 (2012). https://doi.org/10.18434/T4T88K
15. A. I. Popov, V. P. Afanas'ev, A. D. Barinov, Yu. N. Bodisko, A. S. Gryazev, I. N. Miroshnikova, M. Yu. Presnyakov, and M. L. Shupegin, J. Surf. Invest.: X-ray, Synchrotron Neutron Tech. **13**, 832 (2019). https://doi.org/10.1134/S1027451019050124
16. U. Jansson and E. Lewin, Thin Solid Films **536**, 1 (2013). https://doi.org/10.1016/J.TSF.2013.02.019
17. I. Bouabibsa, S. Lamri, and F. Sanchette, Coatings **8**, 370 (2018). https://doi.org/10.3390/coatings8100370
18. A. I. Popov, A. D. Barinov, V. M. Emets, T. S. Chukanova, and M. L. Shupegin, Phys. Solid State **62**, 1780 (2020). https://doi.org/10.1134/S1063783420100261
19. A. Popov, *Disordered Semiconductors: Physics and Applications*, 2nd ed. (Pan Stanford, 2018). https://doi.org/10.1201/b22346
20. T. M. Borisova and R. A. Kastro, Tr. Mosk. Fiz. Tekh. Inst. **5** (1), 21 (2013).

Translated by S. Rostovtseva